IEEE Robotics and Automation Letters (RA-L) paper, presented at ICRA 2026, Vienna, Austria. Cite as RA-L paper.

SPIRA: Small Gas Pipeline Inspection Robot with Spiral Leg-Wheel Mechanism and Single Bending Joint

Mitsuhiro Kamezaki, *IEEE, Member*, Kaoru Yamaguchi, Wen Zhao, Kento Yoshida, Toshitaka Koike, Shota Miyake, and Shigeki Sugano, *IEEE, Fellow*

***Abstract*— Gas pipelines damaged by aging or earthquakes need a robotic system that can quickly inspect 50-mm-diameter service lines, consisting of horizontal and vertical pipes connected by elbow joints, tees, or sockets, from the inside. However, conventional pipe inspection robots do not target 50-mm pipes and various pipe types or lack sufficient speed and a reverse function. Thus, this study develops an in-pipe inspection robot, SPIRA, capable of traveling through 50-mm pipelines while meeting the above requirements. SPIRA has three wheels inclined at 30 degrees to the horizontal, arranged around a cylinder. The cylinder is rotated by a motor around the robot's axis, and the wheels move in a spiral motion while pushing the pipe wall, enabling the robot to move stably and quickly. To overcome socket steps of up to 3 mm and diameter changes in elbow joints, the cylinder and each wheel are connected by a leg with a spring pantograph mechanism. SPIRA has two traveling units linked by a bending joint with a servomotor. When the front and rear parts rotate clockwise (counterclockwise), SPIRA moves forward (backward). When both units rotate in the opposite direction, only the central part of SPIRA rotates on the spot, changing the bending direction so that SPIRA can select any travel direction in a tee. We evaluated the travel performance of SPIRA in a pipeline of horizontal, vertical, elbow joints, tees, or sockets, and found that it could smoothly travel through the pipelines, which is difficult for conventional robot systems to achieve.**

***Index Terms*— Pipe inspection robot, spiral leg wheel, spring pantograph leg, single bending joint, small pipeline**

I. Introduction

GAS pipelines are vital infrastructures supporting our lifelines. Most are buried and are made of carbon steel, which are corroded over time due to exposure to soil and moisture [1]. They are also at risk of damage from loosening joints during earthquakes, strong impacts from heavy machines in civil engineering work, and sandblasting resulting from ruptured water pipes. According to the Gas Safety Office of the Ministry of Economy, Trade and Industry (METI) of Japan, urban gas infrastructure in Japan suffered 1,961 accidents between 2017 and 2021 [2]. Gas leakages caused by these factors not only halt gas supply but also increase the risk of fires or explosions.

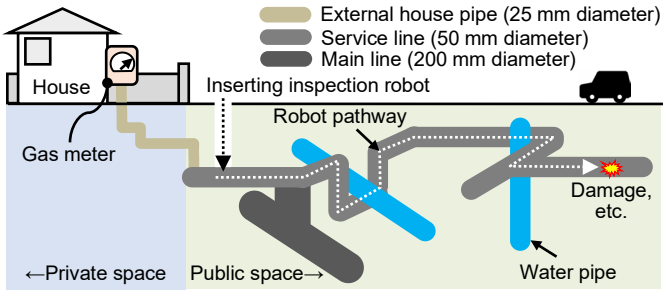

Fig. 1. Robot-assisted gas pipeline inspection in urban areas. Our target is 50 mm diameter pipeline under public road.

Here, we introduce a current recovery procedure when an abnormality occurs. First, human inspectors visit the site and use gas sensors to roughly locate the abnormality by inspecting the road surface. They block off the surrounding traffic and excavate the road using heavy machines, and inspect the inside of the pipeline using a special rigid cable camera [3]. The rigid cable is effective for inserting the camera in straight pipes but does not work for 90° elbow joints, so additional road excavation is required to inspect beyond the elbow joint. Finally, they cut a damaged pipe and replaced it with a new one. However, this method is time-consuming in excavating a road (3 hours) and identifying the damaged area (0.5 hours), incurs high excavation costs, and obstructs smooth road traffic. The current circumstances demand that abnormalities and their conditions be rapidly and reliably estimated at a lower cost, without road excavation, and that long-distance inspection technology capable of handling elbow joints be developed. Thus, to help ensure a safe gas supply, several robot systems for inspecting the inside of pipelines have been developed [4], [5].

There are many types of inspection robots [6], [7], so we first define target pipelines and our robot's requirements. As Fig. 1 shows, gas pipelines consist of main lines (200–300 mm diameter), service lines (50 mm), and house service lines (25 mm), in order from public to private spaces. Accidents on main lines cause extensive damage but occur infrequently, whereas accidents on service lines cause less damage than those on main lines but are more frequent. Gas supply companies are replacing steel pipes with polyethylene (PE) pipes, which are less susceptible to deterioration and more resistant to corrosion and earthquakes [8]. PE-pipe replacement for main lines is prioritized over service lines to reduce series damage, but completion is

Manuscript received June 26, 2025; Revised September 4, 2025; Accepted September 30, 2025. This letter was recommended for publication by Editor Cosimo Della Santina upon evaluation of the reviewers' comments. This work was supported in part by JPNP20004, subsidized by New Energy and Industrial Technology Development Organization (NEDO), Tokyo Gas Network Co., Ltd., and the Future Robotics Organization and Waseda Research Institute Science and Engineering, Waseda University. (*Corresponding author: Mitsuhiro Kamezaki.*)

M. Kamezaki is with the Graduate School of Engineering, The University of Tokyo, 7-3-1 Hongo, Bunkyo-ku, Tokyo 113-8656, Japan, and also with the Future Robotics Organization, Waseda University (e-mail: kamezaki@akg.t.u-tokyo.ac.jp).

K. Yamaguchi, W. Zhao, K. Yoshida, T. Koike, S. Miyake, and S. Sugano are with the Department of Modern Mechanical Engineering, Waseda University, 3-4-1 Okubo, Shinjuku-ku, Tokyo 169-8555, Japan.

Digital Object Identifier (DOI): see top of this page.

TABLE I
COMPARISON OF EXISTING PIPELINE INSPECTION ROBOTS AND OUR ROBOT

Traversal mechanism \ Specifications	Wheel, electric motor [10]	Inch-worm [11]	Pneumatic, inchworm [22]	Peristaltic crawling [23]	Leg-wheel [13]	Crawler [20]	Snake [12]	Wheel legs and bend joint (our study)
Target pipeline diameter [mm]	25	25	✔ 50	✘ 100	✘ 109–129	✘ 136–226	✘ 200	✔ 50
Traversal speed [mm/s]	✘ 6	✘ 6.32	100, 40, 11	✘ 29.2	✔ 500	✔ 230	✔ 120	✔ 100
Travel vertical pipe	✔	n.s.	✔	✔	✔	✔	✔	✔
Travel socket with small step [mm]	✘ 1	n.s.	n.s.	n.s.	(✔)	(✔)	(✔)	✔ 3
Travel elbow joint (curvature) [mm]	✘ R120	✔ R37	✘	✔ 90° elbow	✘ R127.5	✘ R140	✔ 90° elbow	✔ R37
Select path in tees	✔	✔	✘	✘	✔	✘	✔	✔
Travel inversely	✘	✔	✔	✔	✘	✔	✔	✔
Travel long distances	✘	✘	✘	✔	✘	✘	✔ 720 m	(✔)

n.s.: not stated in the paper, ( ): estimated from the experiments

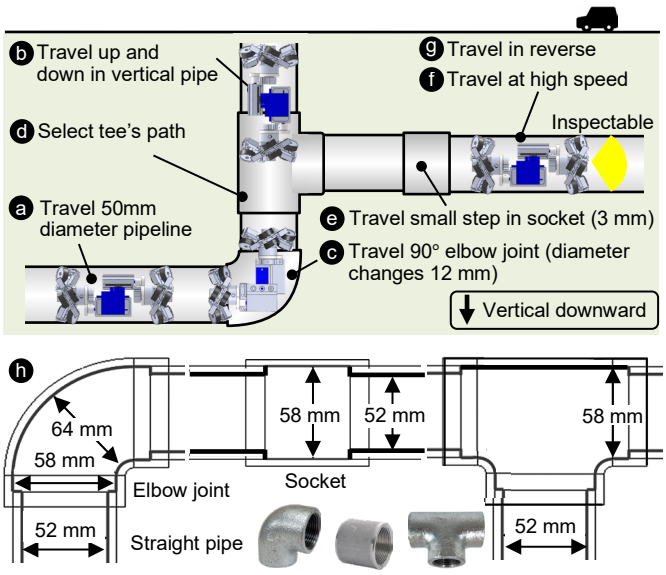

Fig. 2. Requirements for inspection robot. It needs to travel (a) 50 mm diameter pipeline, (b) up and down in vertical pipe, (c) 90° elbow joint, (d) any direction of tee, (e) small step in socket, (f) at high speed, (g) in reverse, and (h) Different diameters in each part of pipeline. The maximum change is 12 (= 64–52) mm .

not expected until around 2040, as Japan's gas supply network extends over 260,000 km [9]. Service lines typically have four bends to avoid water pipes or underground facilities, making inspection difficult. Thus, this study focuses on inspecting service lines by using a robot.

We then summarize the requirements of the inspecting service lines (50 mm diameter), as shown in Fig. 2.

- Travel in 50 mm diameter pipe (a)
- Travel in horizontal and vertical pipes (b)
- Travel 90° elbow joints (curvature radius: R37) (c)
- Select the pass direction at tees (d)
- Pass through sockets with a step (approx. 3 mm) (e)
- Travel at high speed (target speed: 100 mm/s) (f)
- Travel in reverse to retrieve the robot (g)
- Travel long distances (final goal: 30 m)

To begin with the conclusion, no existing robots can satisfy all the requirements listed in Table I. They employ various traveling methods, including wheel [10], inchworm [11], snake [12], crawler [13], or peristaltic types [14]. However, most were designed for main lines of 100 mm or more. Some target service lines of 50 mm but focus on limited pipe movement, such as either vertical or straight pipes, and cannot travel arbitrary pipe networks with elbows and tees. In addition, long-distance travel has not been considered, and travel speeds are as low as 5–6 mm/s. Some robots lack a reverse travel capability.

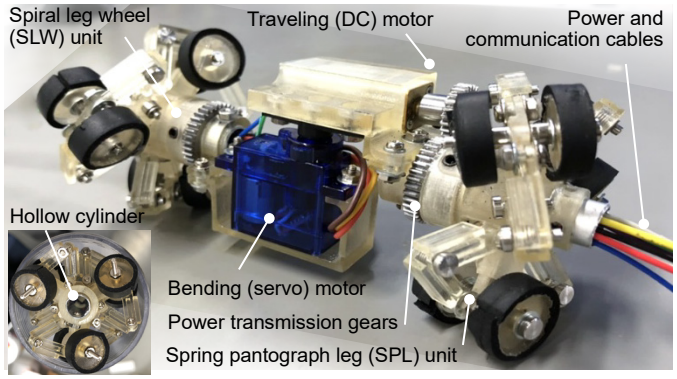

Fig. 3. Overview of SPIRA, which is designed for 50 mm diameter gas pipelines. SPIRA has three motors and 12 wheels in total and can pass through elbow joints, tees, and sockets smoothly. Diameter is normally 65 mm but varies from 52–64 mm due to spring, depending on diameter of pipe elements.

Thus, this study aims to develop a robot that can travel in 50 mm diameter pipelines while satisfying the above indispensable requirements. We call it SPIRA. Specifically, SPIRA has two spiral leg wheel units and one bending joint, as shown in Fig. 3. We evaluated the travel performance of SPIRA in the pipelines. The social significance of this study is to eliminate serious accidents caused by deterioration and damage in critical infrastructure. The industrial significance lies in improving the quality and efficiency of maintenance by introducing robotics safely and inexpensively to the field. The technical significance lies in constructing a design principle and the embodied techniques for a practical small gas pipeline inspection robot.

The rest of the paper is as follows: Section II outlines related and required works, Section III details the development of the SPIRA, and Section IV presents the experimental results and discussion. Section V summarizes the findings of this study.

II. RELATED WORKS

We detail related works on pipeline inspection robots and their mechanisms and then describe the required works. As explained in Section I, various types of robots [15] have been developed to inspect the inside of gas pipes, as listed in Table I. To determine our robot's specifications, we analyze robots with each travel mechanism and their performance.

- *Wheel type*. A 1-inch pipeline robot [10] can travel a 1-inch pipe at 6 mm/s and pick up a 3-mm square object. A spiral-driven pipe inspection robot [13] travels 100−129 mm diameter pipes at 500 mm/s, by rotating its wheels around a rotation axis. They travel only in a forward

direction or have a slow movement speed.

- *Snake type*. MRINSPECT VII+ [12] can travel 200 mm diameter pipes and tees and run in reverse. Explorer [16] can travel 220 mm diameter pipes up to 500 m with a battery and wirelessly communicate. THESBoT-Dual [17] can travel 152.4 mm diameter pipes in all directions at 100 mm/s. However, they cannot travel in small pipelines.
- *Inchworm type.* The inchworm robot using a pneumatic system [11] travels 25 mm diameter pipes, but the speed is slow (7 mm/s). The robot has a pipe-climbing speed of 15.0 mm/s without load for 76–110 mm [18]. A soft in-pipe robot performs multi-locomotion in vertical and horizontal pipes [19], but the speed is also slow (5.8 mm/s).
- *Crawler type*. A multi-module, parallel arrangement type in-pipe inspection robot [20] has three crawlers that can travel inside pipes with 136–226 mm diameter. A cylindrical tracked-crawler can pass elbow joints but not tees. Many types specialize for different purposes, but they all have difficulty satisfying all the requirements.
- *Peristaltic type.* A high-speed propulsion robot [22] using a pneumatic actuator can travel 50 mm diameter pipes at 100, 40, and 11 mm/s for horizontal pipes, vertical pipes, and elbow joints, respectively. A peristaltic robot [23] can travel a consecutive elbow joint of a 1-inch pipe at 4.2 mm/s. This type, however, cannot pass tees.

Again, no existing robots satisfy all the requirements explained in Section I. The above analysis indicates that inchworm and peristaltic types are inherently slow due to their drive principles, crawler types are difficult to miniaturize due to their numerous components, and snake and wheel types have the potential to meet our aim. Snake types generally require many motors, increasing size and complicating control, while wheel types can move at high speed and offer flexibility in wheel arrangement and number. These features would make wheel types more advantageous than snake types in meeting all the above requirements, so in this study, we adopt the wheel type.

III. Design of SPIRA

In this section, we describe the design concept of SPIRA to meet the abovementioned requirements and then explain the mechanisms and functions of each component in detail.

A. Whole design and driving modes

As shown in the requirements in Section I, the robot must travel in any direction and selectively move straight or turn at tees and steps in sockets. Gas pipelines consist of straight pipes (52 mm) connected by elbow joints, tees, and sockets (58 mm), each with a 3 mm step. In an elbow joint, the pipe diameter increases toward the center (in/out: 58 mm, center: 64 mm) (Fig. 2(f)). For stable travel, the wheels must always remain in contact with the pipe wall despite diameter changes and must overcome the steps. The internal space in pipes (52 mm) is quite limited, so the number of motors, which increases the robot size and weight and the number of cables, must be minimized. We thus introduce three minimal driving modes: forward/backward (straight pipes and sockets), bending-direction change, and turning (elbows and tees).

To achieve these driving modes, SPIRA has front and rear

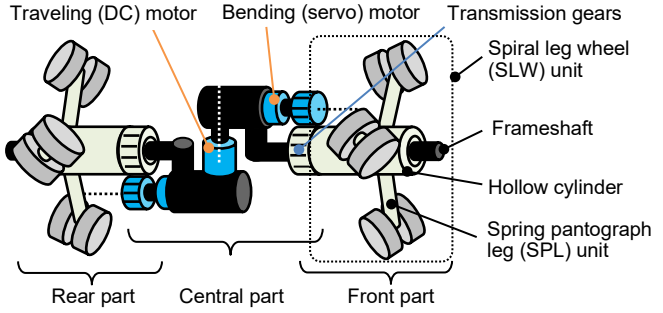

Fig. 4. Simplified schematic SPIRA, consisting of front, central, and rear parts. Two spiral leg wheel (SLW) units are in front and rear parts, and single bending joint (SBJ) is in central part. SLW unit has three wheels and spring pantograph leg (SPL) units to adapt to small steps in sockets and diameter changes in elbow joints. Each SPL unit rotates around frameshaft.

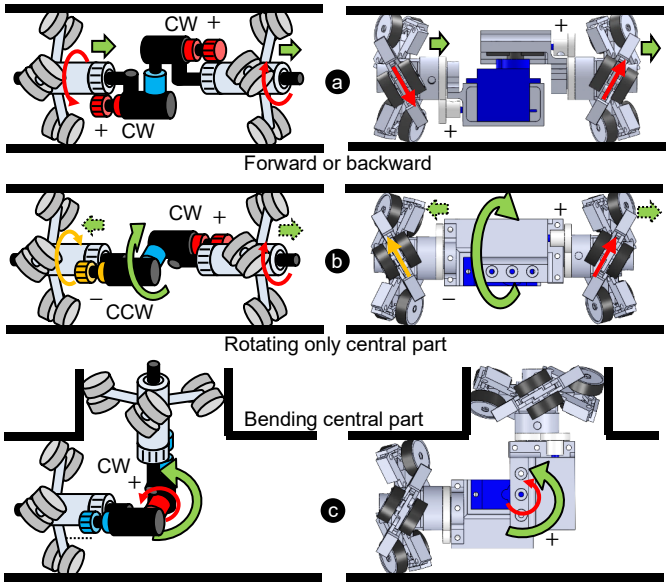

Fig. 5. Three driving modes of SPIRA by adequately compounding three motors' control. Left and right figures show simplified schematic diagram and CAD design, respectively. (a) Traveling forward and backward, (b) adjusting bending direction, and (c) changing traveling direction.

spiral leg wheels (SLWs) with spring pantograph legs (SPLs) and a central part with two DC motors for moving forward/backward and a servomotor for bending (Fig. 4).

- *Spiral leg wheels (SLWs)*. Three wheels are installed at an angle against the direction of the robot's frameshaft and are in contact with the pipe wall. By rotating the SLW around the robot frameshaft, the robot moves forward similarly to how a screw moves forward.
- *Spring pantograph legs (SPLs)*. Each leg for SLWs has a pantograph mechanism using links and springs to apply a suitable pressing force against the pipe walls whose diameters vary and pass through a socket smoothly.
- *Single bending joint (SBJ).* The robot consists of a front, central, and rear parts, and a single bending joint is installed at the central part. By rotating a servomotor in the joint, the robot turns at the elbow joints and tees.

By introducing the abovementioned mechanisms, the robot can achieve the three driving modes by compounding three motors, as shown in Fig. 5.

- *Forward and backward:* When the robot travels a straight pipe forward, it rotates the front and rear SLW units

clockwise (Fig. 5(a)). When traveling backward, the robot rotates the front and rear SLW units in the opposite direction to that of traveling forward.

- *Bending-direction change:* The robot needs to change the bending direction of the servomotor in the direction of elbow joints or tees. The robot changes the bending direction by rotating the front and rear SLW units in the opposite direction (Fig. 5(b)). This motion rotates only the central part around the frameshaft.
- *Turning:* When the robot turns elbow joints and selects a travel direction at tees, it changes the travel direction by rotating the SBJ in accordance with the curvature (Fig. 5(c)). The robot uses composite controls, i.e., traveling forward with two SLW units while rotating the SBJ.

By combining these driving modes, the robot can travel in any direction (up, down, left, or right) with only two motors for forward/backward movement and a single bending joint for direction change and selective travel in a tee. We provide details of the design in subsequent subsections.

B. *Spiral leg wheel (SLW) unit*

1) Structure and mechanism: The SLW enables the robot to move forward and backward by rotating the DC motor around the frameshaft, reducing the number of parts and saving space (Fig. 6(a)). It has three wheel-legs mounted on the hollow cylinder at 120° intervals, with the wheels inclined at φ° to the horizontal (Fig. 6(b)). A larger angle increases travel speed but reduces holding ability and requires higher torque for the SLW unit, while a smaller angle has the opposite effect. How to set φ will be explained later. The hollow cylinder is rotated around the frameshaft by the motor, causing the wheels to follow a spiral path while pushing the pipe wall. Each wheel trajectory results in the robot traveling in the axial direction of the pipe.

2) Assembly of front and rear SLW units: The SLW units are placed at the front and rear to stabilize the robot's posture, particularly during turning [24]. The robot moves forward or backward when the front and rear SLWs rotate clockwise or counterclockwise. In the driving mode, the central part does not rotate. We assemble the two SLW units with opposite spiral directions for two reasons. First, to ease sliding the central part: the frameshaft and hollow cylinder slide in contact with each other, and greater friction causes the central part to rotate. Opposite spiral directions for two SLW units allow the sliding part to release even if sticking occurs. Second, to enhance holding stability: in a vertical pipe, gravity causes each unit to rotate, leading to a fall. Opposite spiral directions act as a brake, preventing the robot from rotating and holding it in its place.

3) Cable routing: The robot needs to receive power and operational signals from outside the pipe, and transmit camera or sensor images to outside the pipe. The SLW units rotate around the frameshaft, so the control, sensor, or power cables must pass through it. We thus designed the frameshaft with a hollow interior (the right upper of Fig. 6(a)), to enable the cables to pass through the robot body. In this study, SPIRA has only control and power cables (seven in total), so we used a hollow cylinder with 8 mm inner diameter. This design also facilitates future multiple robot deployment; for example, the leader robot's cables can pass inside follower robots to avoid entanglement.

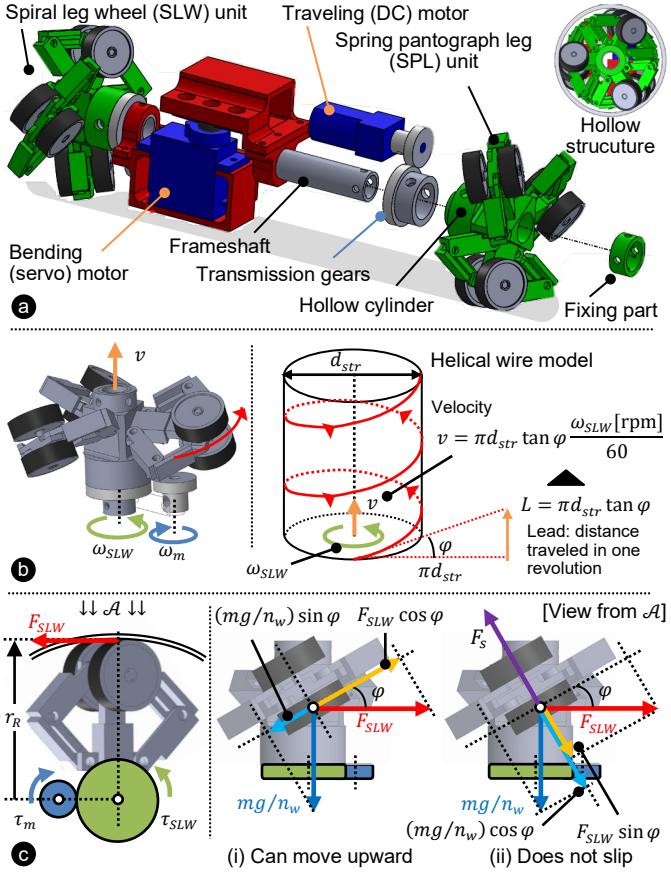

Fig. 6. Design of spiral leg wheel (SLW) unit. (a) Exploded view of SLW unit. (b) Velocity formulation based on spiral trajectory analysis. (c) Torque analysis based on two kinds of equilibrium of force when robot travels vertical pipe upward where the required torque is the largest.

4) Modeling and formulation: Here, we formulate the travel speed and traction force to determine the robot dimensions and the traveling motor. First, from the helical wire model, as shown in Fig. 6(b), the robot travel speed v is calculated by using

$$v = L \cdot \frac{\omega_{SLW}}{60} = \pi d_{str} \tan\varphi \cdot \frac{\omega_{SLW}}{60}\ , \qquad (1)$$

where L is the lead ($= \pi d_{str} \tan\varphi$), d_{str} is the straight pipe diameter (= 52 mm), φ is the wheel inclining angle, and ω_{SLW} is the rotation speed (rpm) of the SLW unit driven by the motor. The robot traction force F generated by the spiral rotation of the SLW unit can be formulated by

$$F = \frac{2\pi \cdot \eta \cdot \tau_{SLW}}{L} = \frac{2 \cdot \eta \cdot \tau_{SLW}}{d_{str} \tan\varphi}\ , \qquad (2)$$

where η is the efficiency of the spiral motion (like a screw) and τ_{SLW} is the torque (N·mm) of the SLW unit. We then formulate the necessary τ_{SLW} to enable the robot to move upward in a vertical straight pipe, which is the most severe situation [25]. As Fig. 6(c) shows, the driving force generated by an SLW unit F_{SLW} is given by $F_{SLW} = \tau_{SLW}/(n_w \cdot r_R)$, where r_R is the distance from the robot center axis to the point where the wheel contacts the pipe wall (= the target pipe's radius) and n_w is the number of wheels in an SLW unit (= 3). The SLW unit can move upward when the component of F_{SLW} in the direction of wheel travel is larger than the component of gravity in that direction (Fig. 6(c,i)), and which is given by

$$\frac{\tau_{SLW}}{n_w \cdot r_R}\cos\varphi > \frac{mg}{n_w}\sin\varphi \;\rightarrow\; \tau_{SLW} > r_R mg\tan\varphi, \quad (3)$$

where m is the robot's mass and g is gravity. Another requirement is that the wheels do not slip during rotation. The wheel legs have springs, so the static friction force is given by $F_s = \mu k l$, where μ is the coefficient of static friction between the pipe wall and wheel, k is the spring constant, and l is the spring's compression length. The robot does not slip when F_s exceeds the sum of the components of F_{SLW} and gravity perpendicular to the wheel movement (Fig. 6(c,ii)), which is given by

$$\mu k l > \frac{\tau_{SLW}}{n_w \cdot r_R}\sin\varphi + \frac{mg}{n_w}\cos\varphi \;\rightarrow\; \tau_{SLW} < r_R\left(\frac{n_w \cdot \mu k l}{\sin\varphi} - \frac{mg}{\tan\varphi}\right). \quad (4)$$

Finally, we obtain the conditional equation,

$$r_R mg\tan\varphi < \tau_{SLW} < r_R\left(\frac{n_w \cdot \mu k l}{\sin\varphi} - \frac{mg}{\tan\varphi}\right). \quad (5)$$

We should determine m, φ, μ, k, l and select the suitable τ_{SLW} that satisfies the above equation for minimizing the robot size. The detailed selection is explained later.

C. Spring pantograph leg (SPL) unit

1) Structure and mechanism: For stable travel, the wheels must always contact the pipe wall despite diameter changes and must overcome steps. Each SLW unit has three legs to stabilize the robot with minimal contact points [26]. As shown in Fig. 7(a), the hollow cylinder and wheels are linked by a pantograph mechanism with a torsion spring at the joint and a guide mechanism. The wheel should extend and retract radially to generate friction, but the pantograph alone cannot move it straight since the endpoint laterally swings. We thus added a guide mechanism to enable straight motion. Moreover, we adopted a double-arm pantograph for greater resistance to external forces. To avoid interference with the pipe or other legs, the wheel is split into two parts with the leg mechanism between them.

2) Modeling and formulation: The force on the wheels by the SPL unit's spring must be set so that the robot can pass various diameter pipes, stop at vertical pipes, and overcome steps in pipes (Fig. 7(b)). To stop in a vertical pipe, the frictional force on the wheels from the spring must exceed the robot's mass (Fig. 7(c)). Assuming that the motor brakes and referring to (4), the conditional equation for one wheel is given by

$$\mu k l > \frac{mg}{n_w}\cos\varphi, \quad (6)$$

Next, to derive a condition for the robot to overcome a step, we analyze the moment when the wheel begins step overcoming and contacts point P, as shown in the left part of Fig. 7(d). The wheel receives the driving force F'_{SLW} from the SLW unit. The driving force F_D for step overcoming is the component of F'_{SLW} in the direction of wheel travel and is given by

$$F_D = F'_{SLW}\cos\varphi = \frac{\tau_{SWL}}{n_w \cdot r_O}\cos\varphi, \quad (7)$$

where r_O is the distance from the robot center axis to point O. The wheel also receives the pressing force F_P from the leg

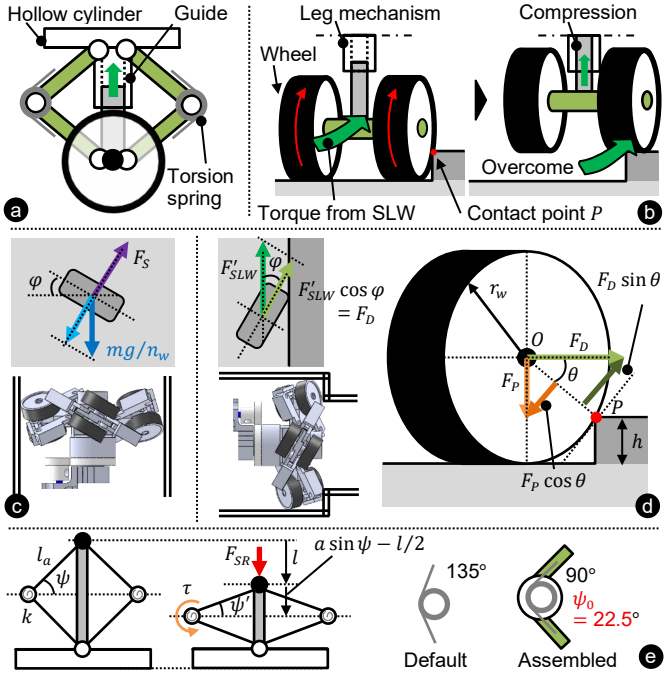

Fig. 7. Design of spring pantograph leg (SPL) unit. (a) Structure of SPL unit. (b) Behavior of step overcoming. Analysis of force exerted on wheel for (c) holding at vertical pipe and (d) step overcoming. (e) Relationship between compression length and repulsive force.

spring, as shown in the right part of Fig. 7(d), and is given by

$$F_P = kl. \quad (8)$$

Assuming that the wheel does not slide when overcoming a step, if the moment of F_D around P is larger than the moment of F_P around P, the wheel can rotate up the step with P as its center of rotation. This can be expressed as $F_D\cos\theta\, r_w > F_P\sin\theta\, r_w$, where r_w is the wheel's radius and θ is the angle between the wheel's axial direction and OP, and is given by

$$\frac{\tau_{SWL}}{n_w \cdot r_O}\cos\varphi\cos\theta > kl\sin\theta. \quad (9)$$

Finally, we obtain the following conditional equation,

$$\frac{mg}{n_w\mu}\cos\varphi \le kl < \frac{\tau_{SWL}\cdot\cos\varphi}{n_w r_O\cdot\tan\theta}, \quad (10)$$

where $\tan\theta = \sqrt{2r_w h - h^2}/(r_w - h)$ and h is the step height (= 3 mm). We should determine k, l, and r_w to meet the above conditions. To end this, we formulate the relationship between compression length l and SPL's repulsive force F_{SR}. As shown in Fig. 7(e), we denote the arm length of the pantograph as a and the initial angle of the arm to the horizontal plane as ψ. When F_{SR} is applied to the wheel (the endpoint of the SPL unit) and it displaces at l, the change in ψ is given by

$$\Delta\psi = \psi - \sin^{-1}\left(\frac{l_a\sin\psi - l/2}{a}\right). \quad (11)$$

The torque exerted by the torsion spring can be obtained by $\tau = k_T\Delta\psi$, where k_T is the spring constant (N·mm/deg). Also, τ can be expressed by $\tau = F_{SR}\cdot l_a\cos\psi$. Thus, the relationship between F_{SR} and x is given by

$$F_{SR} = \frac{k_T}{l_a\cos\psi}\left\{\psi_0 + \psi - \sin^{-1}\left(\frac{l_a\sin\psi - l/2}{l_a}\right)\right\}, \quad (12)$$

where ψ_0 is the pre-compression angle at which the spring is attached to the pantograph mechanism (= 22.5°).

D. Single bending joint (SBJ)

1) Structure and mechanism: The robot needs to travel in any direction and selectively in straight or turning directions for the tees, so it must have a mechanism to actively change its moving direction. Ideally, the robot would have two motors, but saving space and reducing weight are also important. Thus, we implement a single bending joint (SBJ) that enables the robot to turn 0–90° and the bending-direction change mode using front and rear SLW units, as illustrated in Fig. 5(b). The SBJ is a simple structure with a servomotor located in the central part, connecting the front and rear parts, and bends in the center of the robot. Please refer to Fig. 5 to review the turning process.

2) Modeling and formulation: When the front SLW unit enters a straight pipe from an elbow joint, the SPL must be shrunk because the straight pipe diameter (52 mm) is smaller than that of the elbow joint (in/out: 58 mm, center: 64 mm). As Fig. 8(a) shows, the SBJ must generate sufficient torque to compress the spring to its full stroke (= 7.5 mm) by pressing it against the pipe wall. The required torque τ_{SBJ} for the SBJ is given by

$$\tau_{SBJ} > kl_{max}/r_B \ , \tag{13}$$

where r_B is the distance from the rotation center of SBJ to a contact point of the wheel and l_{max} is the full spring stroke.

E. Robot length to pass elbow joint and tee

1) Approach: We integrate the above mechanisms into a robot small enough to pass through pipelines. A robot that is too short or too long cannot pass elbow joints or tees, so we analyze an adequate robot length. SPIRA can be simplified as two T-shaped structures comprising the SLW unit, frameshaft, and SBJ (Fig. 8(b)). The frameshaft diameter d_F (28 mm, the maximum thickness at the central part), the SLW unit length l_{SLW} (15 mm, the wheel unit's width), and the minimum SLW unit distance d_{SLW}^{min} (25 mm, when SPL is fully retracted) are determined by geometric design and various constraints, so we here analyze the frameshaft length l_F.

2) Modeling and derivation: First, we determine the minimum l_F for the robot to pass through an elbow joint stably. To achieve this, either SLW unit should be in a straight pipe. The curvature of the elbow joint is R37, giving l_F > 37 mm. Then, we determine the maximum l_F to avoid interference between the robot body and pipe wall. As shown in Fig. 8(b), when the outer wheel contacts the pipe wall and the SLW unit is fully retracted, the robot can pass through the elbow joint as long as the frameshaft and pipe wall do not interfere at any bending angle α. In Fig. 8(c), the distance d_{FP} between the frameshaft and pipe wall is obtained from geometric calculation, given by

$$d_{FP} = \frac{\left| y_B - \left(\frac{y_C - y_B}{x_C - x_B}\right) \cdot x_B \right|}{\sqrt{\left(\frac{y_C - y_B}{x_C - x_B}\right)^2 + 1}} - r_I \geq 0 \ , \tag{14}$$

where x_i or y_i is the x or y coordinates of point i and r_I is the distance between O and the closest inner wall. We calculate d_{FP} while varying with the combination of α and l_F, and the results indicate that the maximum frameshaft is 46.5 mm. Finally, we obtained the robot length condition, 37 < l_F < 46.5.

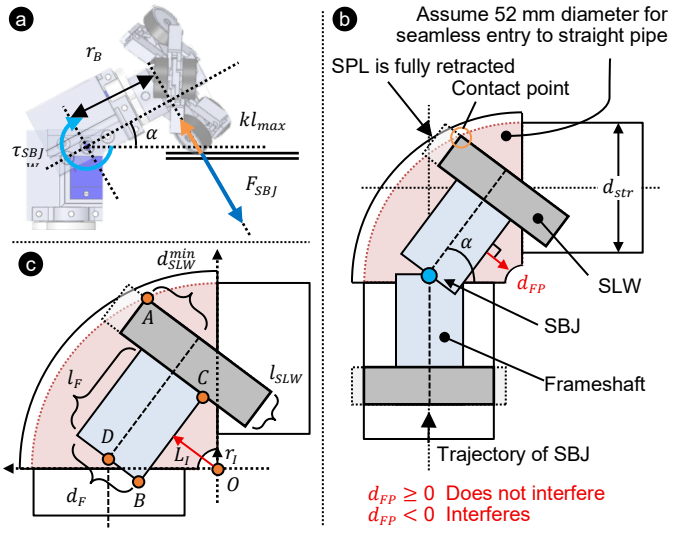

Fig. 8. (a) Torque required for single bending joint. (b) Condition of robot length allowing to pass thorough elbow joint and tee. (c) Geometric calculation of distance between frameshaft and pipe wall.

IV. Prototype Development and Experiments

Based on the design in Section III, we define the specifications to meet the requirements and prototype SPIRA. We then perform fundamental experiments to evaluate its performance and discuss the results, as well as future improvements.

A. Prototype development

Based on the analysis in Section III, we determine the robot parameters to meet the requirements mentioned in Section I. The number of parameter combinations to be searched is quite large, making the grid search and analytical deviation methods impractical. Thus, we first iteratively determine the dimensions of each part of the robot, including selecting two types of motors, and then verify whether the design satisfies the conditional equations (1), (2), (5), (10), (13), and (14).

1) Design parameters: The primary dimensions of the parts are listed in Table II. To balance travel speed and holding stability, we set φ = 30°. We selected the torsion spring of 0.11 N·mm/deg (T006B/TL006B, Misumi). The robot must adapt to 52–64 mm diameter pipes, so we set the SPL stroke to 7.5 mm (compression length at straight pipe l is 6.5 mm) so that d_{SLW} varies between 50–65 mm. We set l_F to 40 mm, satisfying the length requirement. To satisfy torque, speed, and size the requirements, we selected a N20 (Bringsmart) as the traveling DC motor, with rated torque of 98.1 N·mm and speed of 160 rpm. We implemented a power transmission gear with a gear ratio of 12:18. We also selected MG90D (TowerPro) as the bending servomotor motor, with rated torque of 235.4 N·mm and speed of 0.48 rev/s. We adopted η of 0.4 by referring to sliding screws.

2) Verification of specifications: As listed in Table III, all derived specifications meet the requirements. Our ω_{SLW} is 106.7 rpm (= ω_m/α), giving v = 167.7 mm/s from (1), exceeding the required 100 mm/s. From (5), the required τ_{SLW} range is 22.05–151.8 N·mm, and ours is 147.2 N·mm (=$\tau_m \cdot \alpha$), satisfying the

TABLE II
DESIGN PARAMETERS OF SPIRA

D	Target pipe diameter	52–64 mm
h	Height of step	3 mm
l_R	Length of robot	116 mm
l_F	Length of frameshaft	40 mm
d_F	Diameter of frameshaft	28 mm
l_{SLW}	Length of SLW	15 mm
d_{SLW}	Diameter of SLW (minimum and maximum)	50–65 mm
r_w	Wheel radius	7.5 mm
l_a	Arm length of SPL	13.5 mm
φ	Inclination angle of wheel	30°
l	Compression length at straight pipe	6.5 mm
k_T	Spring constant for SPL	0.11 N·mm/deg
μ	Friction coefficient b/w pipe wall and wheel	0.6 (steel & rubber)
η	Efficiency of spiral motion	0.4 (sliding screw)
α	Gear ratio	18:12
m	Mass of robot	150 g

TABLE III
SPECIFICATIONS OF SPIRA

		Condition	Selected
ω_{SLW}	Rotation speed of SLW (no load)	–	106.6 rpm
τ_{SLW}	Torque of SLW (no load)	22.05–151.8	147.2 N·mm
ω_{SBJ}	Rotation speed of SBJ (no load)	–	28.8 rpm
τ_{SBJ}	Torque of SBJ (no load)	> 20.85	235.4 N·mm
kl	Repulsive force of SPL	0.7072–3.776	0.9149 N
v	Theoretical speed of robot	> 100	167.7 mm/s
F	Traction force of robot (payload)	–	3.929 N

condition. From (10), the required kl range is 0.7072–3.776 N, and ours is 0.9149, satisfying the condition. From (13) and r_B = 46.5 mm, τ_{SBJ} must exceed 20.85 N·mm, satisfied by our 235.4 N·mm. From (2), the theoretical payload is 392.9 g.

In this study, we mainly used resin for structural components and fabricated them using a 3D printer, which can make complex parts and make the robot lighter (Fig. 1).

B. Experiments

The aim of the experiments is to verify whether SPIRA satisfies the requirements in Section I under the minimum necessary environmental conditions, rather than through an extensive field evaluation. For ease of manual control and video recording, we used rigid polyvinyl chloride (PVC) straight pipes and tees (μ w/ rubber ≈ 0.35) and cast-iron elbow joints and sockets (μ w/ rubber ≈ 0.6). The pipe interiors were dry and free from corrosion, dust, and lubrication. Fig. 9 shows the results of movement experiments in (a) a horizontal straight pipe, (b) a vertical straight pipe, (c) a socket in a straight pipe, (d) a 90° elbow joint, (e) passing straight at a tee, and (f) turning at a tee. SPIRA could travel in both forward and reverse directions in the straight pipes by switching the rotation direction of the traveling motors and moved smoothly in elbow joints, tees, and sockets.

Each condition was tested 10 times, with all trials completed successfully. The robot's speed was calculated from video frames with a scale placed beside the pipe and averaged across trials, with no detectable variation observed. Table IV shows that the horizontal forward and reverse (both 210 mm/s), vertical upward (200 mm/s), and vertical downward speeds (245 mm/s) all exceed the requirements. The payload was then measured under the most severe condition, i.e., vertical upward movement. A weight was attached to the robot with a string, and we repeatedly determined the maximum load that allowed the target speed of 100 mm/s. The result was 430 g, almost the same as the designed value and sufficient to install sensors, such as a camera, in the future. Although the evaluation experiments are simple and fundamental, they confirm that SPIRA satisfies the requirements.

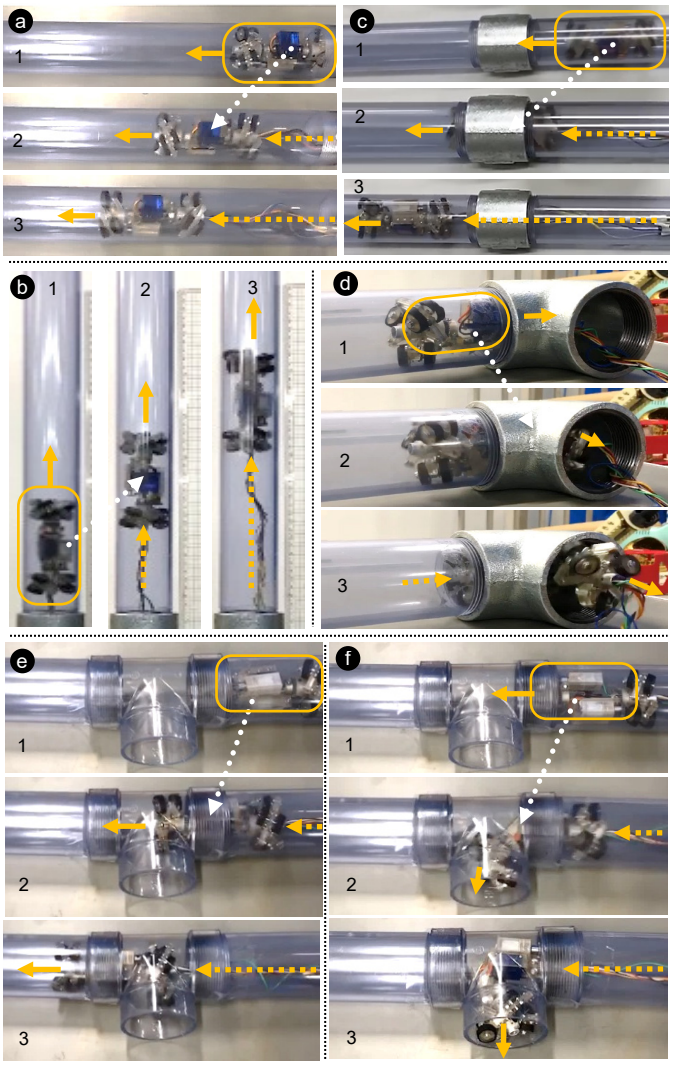

Fig. 9. Movement experiments using manually controlled SPIRA. Tasks include (a) horizontal straight pipe, (b) vertical straight pipe, (c) socket (3 mm inside step), (d) 90° elbow joint, (e) passing straight at tee, and (f) turning at tee. SPIRA successfully passed through all pipes.

TABLE IV
FUNDAMENTAL ROBOT PERFORMANCE

Average horizontal forward and reverse speed	210 mm/s, 210 mm/s
Average vertical upward and downward speed	200 mm/s, 245 mm/s
Payload while moving vertically upward	430 g

* In experiments, speeds at elbow joint and tee were not measured since they are largely affected skills in manual operation.

C. Future improvements

SPIRA is a prototype robot designed to evaluate mechanisms and design methods, so we identified room for improvement.

1) Evaluation in more realistic conditions: We need to evaluate the performance under conditions commonly presented in field pipelines, such as humidity, dust, debris, corroded or uneven surfaces, and the influence of long tether drag on navigation and stability. To operate in these conditions, for example, softer wheels may be needed to increase the contact area to enhance grip. Moreover, we should have tested the robot in gas-filled environments. To achieve this, we must introduce several

designs, including an explosion-proof design that uses brushless DC motors and isolates the electric circuit boards outside the pipe and a waterproof design that encloses electric components in a box and seals the electric wires with glue.

2) Robot structure: The prototype design focused on the part's size, functional mechanisms, and performance of the robot. For ease of fabrication, we made it from resin using a 3D printer. However, resin construction is inferior to metal in smooth sliding, strength, and durability. In the experiments, the central part rotated during forward and reverse movements, due to differences in friction and rotational speed between the front and rear SLW units. To address this, we will apply speed synchronization control or a small wheel contacting the inner pipe wall to stabilize posture. Future development will employ metal materials, taking into account the increased mass of the robot.

3) Automatic control: In this study, we directly saw SPIRA in a pipe and controlled it manually. However, in real scenarios, we cannot see the robot directly, so we need to implement an automatic control system, e.g., [27]. To achieve this, we will implement a sensor system that includes wide-angle cameras at the front and rear ends of the frameshaft or inertial measurement units at the center of front and rear parts. Currently, passing elbow joints and tees takes time, so a sensor-based automatic control system is highly desirable.

V. Conclusion

In this study, we developed SPIRA, a principal prototype of small (50 mm diameter) gas pipeline inspection robots capable of inspecting a pipeline consisting of horizontal and vertical pipes, elbow joints, tees, and sockets. SPIRA features unique mechanisms, including spiral leg wheel (SLW) units, spring pantograph leg (SPL) units, and single bending joint (SBJ). By combining three driving modes, the robot can travel in any direction, i.e., up, down, left, or right, with only two motors for forward or backward movement and a single bending joint for direction changes and selective travel in a tee. In travel experiments, SPIRA achieved stable, high-speeds motion in both horizontal and vertical pipes using SLW units. In step-overcoming test, the SPL units prevented the robot from getting stuck at steps in sockets, elbow joints, and tees. The SBJ also enabled smooth direction changes in elbow joints and tees. The proposed design contributes to achieving a compact size and high-speed travel while reducing the number of motors, previously a challenge for wheel-type robots, and still enabling the incorporation of a bending joint.

In the future, we evaluate SPIRA under more realistic conditions. We also plan to implement an automatic control system to enable smoother travel through elbow joints and tees, and to incorporate explosion-proof designs by updating each mechanism. Moreover, we will investigate the scalability of the proposed design, with a particular focus on smaller-diameter pipes.

References

[1] M.V. Biezma, M.A. Andrés, D. Agudo, E. Briz, "Most fatal oil & gas pipeline accidents through history: A lessons learned approach," *Engineering Failure Analysis*, vol. 110, p. 104449, 2020.

[2] Gas Safety Office, METI, Japan, "City gas accident." [Online]. Available: https://www.meti.go.jp/shingikai/sankoshin/hoan_shohi/gas_anzen/pdf/025_s01_00.pdf

[3] T. Tsubouchi, S. Takaki, Y. Kawaguchi, and S. Yuta, "A straight pipe observation from the inside by laser spot array and a TV camera," in *Proc. IEEE/RSJ Int. Conf. Intell. Rob. Syst.*, pp. 82–87, 2000.

[4] Y. Du, Q.M. Zhu, S. Ghauri, J.-H. Zhai, H.-R. Jia, and H. Nour, "Progresses in study of pipeline robot," in *Proc. Int. Conf. Modelling, Identification and Control*, pp. 808–813, 2012.

[5] S. Roh and H. R. Choi, "Differential-drive in-pipe robot for moving inside urban gas pipelines," *IEEE Trans. Rob.*, vol. 21, no. 1, pp. 1–17, 2005.

[6] S. Miyake, K. Yoshida, S Sugano, and M. Kamezaki, "Preliminary design and evaluation of a ducted-fan type pipeline robot," *ROBOMECH J.*, vol. 11, no. 17, pp. 1–10, 2024.

[7] W. Zheng, X. Jiang, M. Kamezaki, C. Tai, P. Zhang, T. Miyake, S. Miyake, X. Liu, Y. Nakatsuka and S. Sugano, "Prototype design of a multi-mode switching module with locking mechanism for water-proof pipeline inspection robots," in *Proc. IEEE/SICE Int. Symp. Syst. Integration*, pp. 741–746, 2024.

[8] T. Bachir-Bey and N. Belhaneche-Bensemra, "Investigation of polyethylene pipeline behavior after 30 years of use in gas distribution network," *J. Materi. Eng. Perform.*, vol. 29, pp. 6652–6660, 2020.

[9] Japan Natural Gas Security Policy, [Online]. Available: https://www.iea.org/articles/japan-natural-gas-security-policy

[10] K. Suzumori, T. Miyagawa, M. Kimura, and Y. Hasegawa, "Micro inspection robot for 1-in pipes," *IEEE/ASME Trans. Mechatron.*, vol. 4, no. 3, pp. 286–292, 1999.

[11] Y. Shen et al., "Design of a pneumatically driven inchworm-like gas pipe inspection robot with autonomous control," in *Proc. IEEE Int. Conf. Soft Robotics*, pp. 1–6, 2023.

[12] H. Jang, H. M. Kim, M. S. Lee, et al., "Development of modularized in-pipe inspection robotic system: MRINSPECT VII+," *Robotica*, vol. 40, no. 5, pp. 1361–1384, 2022.

[13] A. Kakogawa, T. Nishimura, and S. Ma, "Designing arm length of a screw drive in-pipe robot for climbing vertically positioned bent pipes," *Robotica*, vol. 34, no. 2, pp. 306–327, 2016.

[14] T. Kishi, M. Ikeuchi, and T. Nakamura, "Development of a peristaltic crawling inspection robot development of a peristaltic crawling inspection robot for 1-inch gas pipes with continuous elbows," in *Proc. IEEE/RSJ Int. Conf. Intell. Rob. Syst.*, pp. 3297–3302, 2013.

[15] A. Verma, A. Kaiwart, N. D. Dubey, F. Naseer, and S. Pradhan, "A review on various types of in-pipe inspection robot," *Materials Today: Proceedings*, vol. 50, no. 5, pp. 1425–1434, 2022.

[16] H. Schempf, E. Mutschler, A. Gavaert, G. Skoptsov, and W. Crowley, "Visual and nondestructive evaluation inspection of live gas mains using the explorer™ family of pipe robots," *J. Field Rob.*, vol. 27, no. 3, pp. 217–249, 2010.

[17] HiBot, "THESBOT-DUAL." [Online]. Available: https://www.hibot.co.jp/products/thes-dual/.

[18] W. Wang et al., "A modular soft pipe-climbing robot with high maneuverability," *IEEE/ASME Trans. Mechatron*., early access, pp. 1–10, 2024.

[19] C.-Y. Yeh, C.-Y. Chen, and J.-Y. Juang, "Soft hopping and crawling robot for in-pipe traveling," *Extreme Mechanics Letters*, vol. 39, pp 1–8, 2020.

[20] A. Kakogawa, S. Ma, and S. Hirose, "An in-pipe robot with underactuated parallelogram crawler modules," in *Proc. IEEE Int. Conf. Rob. Autom.*, pp. 1687–1692, 2014.

[21] J. Nagase and F. Fukunaga, "Development of a novel crawler mechanism for pipe inspection," in *Proc. Annual Conf. IEEE Industrial Electronics Society*, pp. 5873–5878, 2016.

[22] T. Yamamoto, M. Konyo, and S. Tadokoro, "A high-speed locomotion mechanism using pneumatic hollow-shaft actuators for in-pipe robots," in *Proc. IEEE/RSJ Int. Conf. Intell. Rob. Syst.*, pp. 4724–4730, 2015.

[23] T. Tomita, T. Tanaka, and T. Nakamura, "Development of a peristaltic crawling robot for long-distance sewer pipe inspection with consideration of complex pipe line," in *Proc. IEEE/RSJ Int. Conf. Intell. Rob. Syst.*, pp. 2742–2747, 2015.

[24] T. Zheng, X. Wang, H. Li, C. Zhao, Z. Jiang, Q. Huang, and M. Ceccarelli, "Design of a robot for inspecting the multishape pipeline systems," *IEEE/ASME Trans. Mechatron.*, vol. 27, no. 6, pp. 4608–4618, 2022.

[25] A. Kakogawa and S. Ma, "Stiffness design of springs for a screw drive in-pipe robot to pass through curved pipes and vertical straight pipes," *Adv. Robot.*, vol. 26, no. 3–4, pp. 253–276, 2012.

[26] H. M. Kim, Y. S. Choi, Y. G. Lee, and H. R. Choi, "Novel mechanism for in-pipe robot based on a multiaxial differential gear mechanism," *IEEE/ASME Trans. Mechatron.*, vol. 22, no. 1, pp. 227–235, 2017.

[27] M. Karkoub, O. Bouhali, and A. Sheharyar, "Gas pipeline inspection using autonomous robots with omni-directional cameras," *IEEE Sensors J.*, vol. 21, no. 14, pp. 15544–15553, 2021.